

Aerial and Grounding System Analysis by the Shifting Complex Images Method

Roberto Andolfato, Luca Bernardi, and Lorenzo Fellin, *Member, IEEE*

Abstract—This paper introduces a novel computer method for the analysis of both aerial and grounding systems of conductors. The computer method based on an hybrid approach, allows to incorporate into a single linear system both lumped and distributed circuit parameters, evaluated by a rigorous electromagnetic field analysis. The conductor system is replaced by a suitable set of elementary current sources. These may be plain or hollow, bare or insulated, freely oriented and interconnected in the three dimensional space, which is considered formed by two half spaces each one homogeneous, linear and isotropic (e.g., air and soil). Therefore the method does not pose geometric and topological limitations and enables to compute voltages and currents at the source (boundary) elements as well as vector potentials, electric and magnetic fields anywhere in the surrounding medium. The range of application of this method is sufficiently wide including any practical electric power system application. The method may be applied for frequencies up to 1 MHz, thus covering the frequency spectrum of a typical full lightning too. Results which are derived first in the frequency domain can be converted to the time domain by Fourier Transform algorithms. In this way it is also possible to analyze the response to transient signals of both aerial and grounding systems having complex geometry.

Index Terms—Capacitive coupling, computer modeling, conductive coupling, distribution systems, electromagnetic field, electromagnetic interference, grounding systems, inductive coupling, safety.

I. INTRODUCTION

ELECTROMAGNETIC field computation cannot be considered a standard procedure, since the suitable numeric method has to be selected depending on the specific problem. An integral method is introduced in this work: it is particularly advantageous to solve linear problems in open region: as compared with differential ones, it reduces both the number of unknowns and the computation efforts; the discretization of source surfaces is necessary only in the pre-processing work and the field analysis can be extended in the whole space. On the contrary, the use of integral methods needs greater efforts to obtain analytical expressions for the computation of electromagnetic quantities by means of integrals extended to the elementary sources surface. Every effort in this phase is plentifully rewarded in terms of reducing the computation time.

The method proposed involves other well known numerical procedures like the Method of Moment to change from analytical to numerical approach and the Images Method to consider the difference of electrical characteristics between air and soil

for the computation of electrostatic component of electromagnetic field.

To solve the same problem for the computation of inductive component of electromagnetic field the Shifting Complex Images Method (SCIM) is introduced which interprets Sommerfeld's integrals in terms of images.

By SCIM it is possible to select the complex image number depending on frequency and computation precision required. Furthermore, the solution of the problem in terms of images, once analytical expressions for scalar and vector potentials and electric and magnetic fields due to a single elementary source are known, gives a simple way to obtain any electromagnetic quantities in any point of the propagation medium by applying superposition method.

II. MATHEMATICAL MODEL

Every electromagnetic phenomenon may be described by the well known set of Maxwell equations, normally written using electric and magnetic field. However the same equations may be written using scalar and vector potentials. For a linear and isotropic medium, considering an harmonic state, Maxwell equations in a matricial notation are of the form:

$$\{\Delta, -\dot{\gamma}^2\} \begin{bmatrix} \dot{\mathbf{A}} \\ \dot{\mathbf{V}} \end{bmatrix} = \begin{bmatrix} -\mu \dot{\mathbf{J}} \\ -\dot{q}/\dot{\epsilon} \end{bmatrix} \quad (1)$$

where $\dot{\gamma} = \sqrt{j\omega\mu\dot{\sigma}}$ represents the propagation constant of the medium while q and \mathbf{J} represent charge and current density distribution on the field sources respectively. Furthermore, $\dot{\sigma} = \sigma + j\omega\epsilon$ and $\dot{\epsilon} = \epsilon + \sigma/j\omega$ indicate the complex conductivity and complex permittivity of the medium respectively.

Solutions of (1) are given by the following equations:

$$\dot{\mathbf{A}} = \frac{\mu}{4\pi} \int_{V_j} \frac{\dot{\mathbf{J}} e^{-\dot{\gamma}r}}{r} dv \quad (2a)$$

$$\dot{\mathbf{V}} = \frac{1}{4\pi\dot{\epsilon}} \int_{V_q} \frac{\dot{q} e^{-\dot{\gamma}r}}{r} dv \quad (2b)$$

where V_j and V_q are the space regions where current and charge density distributions exist.

If currents and charges are bordered in thin conductors, equations (2) can be replaced by the following equivalent equations:

$$\dot{\mathbf{A}} = \frac{\mu}{4\pi} \int_L \frac{\dot{I} e^{-\dot{\gamma}r}}{r} dl \quad (3a)$$

$$\dot{\mathbf{V}} = \frac{1}{4\pi\dot{\epsilon}} \int_L \frac{\dot{q} e^{-\dot{\gamma}r}}{r} dl \quad (3b)$$

Manuscript received April 27, 1999; revised February 1, 2000.

The authors are with the Department of Electrical Engineering, University of Padova - Italy.

Publisher Item Identifier S 0885-8977(00)07214-9.

where L represents the conductor length and l the coordinate along its axis.

The relation between charge and current distributions is $\dot{q} = j\dot{s}/\omega$ where $\dot{s} = d\dot{I}/dl$.

Electric and magnetic fields can be calculated as:

$$\dot{\mathbf{E}} = -\text{grad } \dot{V} - j\omega\dot{\mathbf{A}} \quad (4a)$$

$$\dot{\mathbf{H}} = \frac{1}{\mu} \text{rot } \dot{\mathbf{A}} \quad (4b)$$

where vector and scalar potentials are given by (3)

If the complex conductivity of the source material is much greater than that of the surrounding medium, the current distribution along the generic conductors is given by the following expression:

$$\dot{z}\dot{I} + \frac{\partial \dot{V}}{\partial l} + j\omega\dot{A} = \dot{0} \quad (5)$$

where \dot{z} is the internal impedance per unit length of the conductor, \dot{V} and \dot{A} are the axial component of the vector potential and the scalar potential on surface of the conductor respectively.

Generally (5) can be solved only using a numerical approach. Dividing the whole conductor system into n segments (elementary sources), each one having a length L_k , much smaller than the dimension of conductor network, equation (5), for the segment k , gives:

$$\dot{z}_k\dot{I}_k + \sum_{i=1}^n \frac{\partial \dot{V}_{ik}}{\partial l} + j\omega \sum_{i=1}^n \dot{A}_{ik} = \dot{0} \quad (6)$$

where \dot{I}_k is the longitudinal current.

The integration of (6) along L_k yields:

$$\int_{L_k} \dot{z}_k \dot{I}_k dl + \sum_{i=1}^n \int_{L_k} \frac{\partial \dot{V}_{ik}}{\partial l} dl + j\omega \sum_{i=1}^n \int_{L_k} \dot{A}_{ik} dl = \dot{0}. \quad (7)$$

If L_k is sufficiently small, the longitudinal and transversal (leakage) current on both right and left half segments can be assumed to be uniform and equal to their average value. Then $\bar{I}_{kl} = \dot{I}_{kl} - \dot{S}_k/4$ for $0 \leq l < L_k/2$ and $\bar{I}_{kr} = \dot{I}_{kr} + \dot{S}_k/4$ for $L_k/2 < l \leq L_k$ where \dot{S}_k , \dot{I}_l , \dot{I}_r are the total leakage current and left and right-endpoint current of the segment. The situation is well represented in Fig. 1

With such assumptions, the integration of (7) along L_k for left and right half segments yields respectively:

$$\dot{z}_k \frac{L_k}{2} \bar{I}_{kl} + \sum_{i=1}^n [\dot{V}_{ikc} - \dot{V}_{ikl}] + \sum_{i=1}^n [\dot{M}_{ilk} \bar{I}_{il} + \dot{M}_{irk} \bar{I}_{ir}] = \dot{0} \quad (8)$$

$$\dot{z}_k \frac{L_k}{2} \bar{I}_{kr} + \sum_{i=1}^n [\dot{V}_{ikr} - \dot{V}_{ikc}] + \sum_{i=1}^n [\dot{M}_{ikr} \bar{I}_{il} + \dot{M}_{irk} \bar{I}_{ir}] = \dot{0} \quad (9)$$

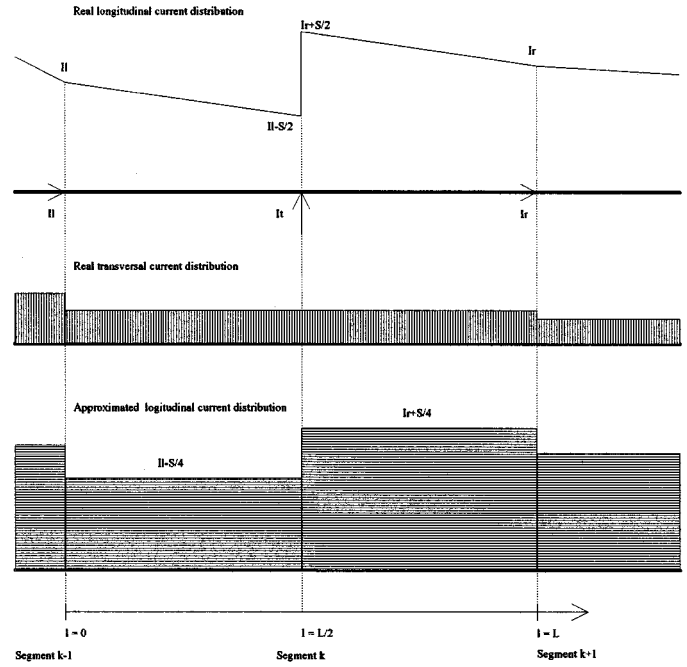


Fig. 1. Approximate current distribution in an elementary source.

where the mutual inductive impedance \dot{M}_{ij} is given by the following equation:

$$\dot{M}_{ij} = j\omega \dot{L}_{ij} = \frac{j\omega}{\dot{I}_i} \int_{L_j} \dot{A}_{ij} dl. \quad (10)$$

As regards whole conductor network equations (8) and (9) can be rewritten in matrix equivalent form as:

$$\begin{bmatrix} [\dot{Z}_{ll}] & [\dot{Z}_{lr}] \\ [\dot{Z}_{rl}] & [\dot{Z}_{rr}] \end{bmatrix} \begin{bmatrix} \{\dot{I}_l\} \\ \{\dot{I}_r\} \end{bmatrix} = \begin{bmatrix} [\dot{Z}_{lt}] & \{\dot{I}_t\} \\ [\dot{Z}_{rt}] & \{\dot{I}_t\} \end{bmatrix} \quad (11)$$

where \dot{I}_t represents the injected current in the middle point of the segment (see Fig. 1). Furthermore, the first Kirchoff's law applied to every segment of the system holds:

$$\{\dot{S}\} = \{\dot{I}_l\} - \{\dot{I}_r\} + \{\dot{I}_t\}. \quad (12)$$

Coefficients of (11) are a linear combination of internal impedance, mutual inductive coupling impedance and mutual capacitive and conductive coupling impedance (see Section III). Equation (11) contains all the information about geometric and physical characteristics of the field sources and of the propagation medium. Its solution gives endpoint currents of each elementary segment and the leakage current can be easily computed by (12). Electric and magnetic fields can be obtained from the longitudinal and transversal current, anywhere in the medium, applying the superposition of the effects of the single elementary source.

The number of unknowns in (11) can be reduced by introducing topologic relationships for the conductor network: where connections point between only two segment are predominant, the number of unknown is just greater than n .

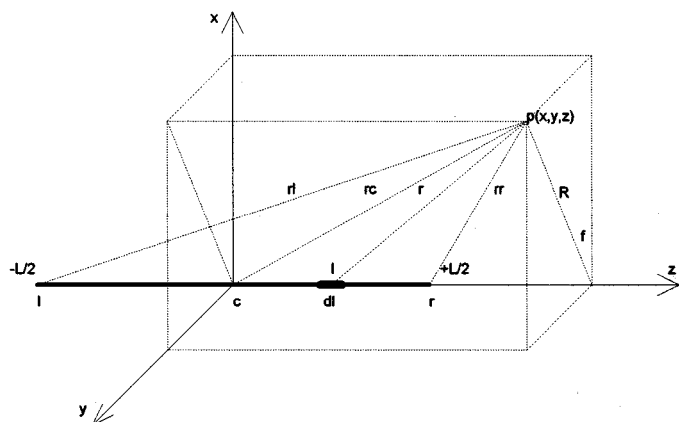


Fig. 2. Coordinate system.

III. PARAMETERS OF THE MODEL

Coefficients of (11) can be obtained from the expression of the internal impedance of a segment per unit length, the mutual capacitive-conductive coupling coefficient between source and a generic point and the mutual inductive coupling coefficient between two sources.

A. Internal Impedance of an Elementary Source

Internal impedance of a generic source represents the lost power and the variations of the amount of electromagnetic energy stored inside the conductor.

Internal impedance of a metallic cylindrical tube can be computed by using the following equation [1]:

$$\dot{z}_i = \frac{j\omega\mu_c}{2\pi r_0 \dot{\gamma}_c} \frac{I_0(\dot{\gamma}_c r_0) K_1(\dot{\gamma}_c r'_0) + K_0(\dot{\gamma}_c r_0) I_1(\dot{\gamma}_c r'_0)}{I_1(\dot{\gamma}_c r_0) K_1(\dot{\gamma}_c r'_0) - I_1(\dot{\gamma}_c r'_0) K_1(\dot{\gamma}_c r_0)} \quad (13)$$

where r_0 and r'_0 are the outer and inner radius respectively, $\dot{\gamma}_c$ is the propagation coefficient, I_n and k_n are the modified Bessel functions of order n of the first and second kind.

B. Coefficient of the Mutual Capacitive-Conductive Coupling

The mutual capacitive-conductive coupling coefficient between source and a generic point (p) represents the ratio between the scalar potential generated from the source in (p) and the leakage current from the whole source.

Let $\dot{\rho} = 1/\dot{\sigma}$ be the complex resistivity. If the coordinate system shown in Fig. 2 is assumed, the application of (3b) in the case of a short conductor segment (elementary source) which leaks current uniformly in the surrounding medium and in the case of point-source, both located in an infinity, homogeneous, isotropic and linear medium, leads to the following equations respectively:

$$\dot{V} = \dot{\rho} \dot{S} \Psi \quad (14a)$$

$$\dot{V} = \dot{\rho} \dot{S} \psi \quad (14b)$$

where

$$\Psi = \frac{1}{4\pi L} \int_L \frac{e^{-\dot{\gamma} r}}{r} dl \quad (15a)$$

$$\psi = \frac{1}{4\pi} \frac{e^{-\dot{\gamma} r}}{r}. \quad (15b)$$

Equations (14a) and (14b) allow to obtain the scalar potential due to both leakage current \dot{S} from the elementary source along its total length and currents $\dot{I}_l e^{\dot{I}_r}$ flowing at the source end-point.

Let us suppose a medium composed by two homogeneous isotropic and linear half spaces separated by a plane Σ and assume the following symbology:

- n indicates the half space in which the source is located;
- j indicates the opposite half space;
- m indicates the half space containing the observation point;
- i indicates the opposite half space.

Be $\dot{v} = (\dot{\rho}_j - \dot{\rho}_n)/(\dot{\rho}_j + \dot{\rho}_n)$ and δ_{mn} the reflection coefficient corresponding to medium n and medium j and the Kronecker's delta respectively.

Expressions of the mutual capacitive-conductive coupling coefficient both between conductor segment and a generic point and between a point-source and a generic point may be obtained using the Images Method (IM) and equations (14a) and (14b).

Such expressions assume the following forms respectively:

$$\dot{K} = \dot{\rho}_m [(1 - \dot{v} + \dot{v} \delta_{mn}) \Psi + \dot{v} \delta_{mn} \Psi'] \quad (16a)$$

$$\dot{k} = \dot{\rho}_m [(1 - \dot{v} + \dot{v} \delta_{mn}) \psi + \dot{v} \delta_{mn} \psi'] \quad (16b)$$

where the quantities marked with superscript indicate contributions of image sources.

The computation of the mutual capacitive-conductive coupling coefficient requires some tricks when sources are coated or in other particular cases, for example when the reference point for the computation corresponds to a node which connects two or more sources or when it lies on Σ .

By coefficients \dot{k} the linear system (11) contains information about the topology of the conductor network.

C. Coefficient of the Mutual Inductive Coupling

The mutual inductive coupling coefficient between two generic sources is defined by (8).

Consider the coordinate system shown in Fig. 2 and suppose an infinity, homogeneous, isotropic and linear medium: if the longitudinal current is assumed to be constant along the elementary source, then (3a) can be rewritten as:

$$\dot{A} = \mu \dot{I} L \Psi \frac{z}{z} \quad (17)$$

where Ψ is given by (15a).

Let us consider the particular coordinate system shown in Fig. 3 (in which the source is located on the plane $Y = 0$ without any loss of generality) and suppose a medium composed by two homogeneous isotropic and linear half spaces separated by a plane Σ .

In this case, using the symbology introduced above and indicating with 1 and 2 soil layer and air layer respectively, horizontal and vertical components of the vector potential generated by an elementary segment can be written as follows:

$$\dot{A}_X = \frac{\mu_m \cos \beta}{4\pi} \int_L [(g_m - g'_m) \delta_{mn} + U] \dot{I} dl \quad (18)$$

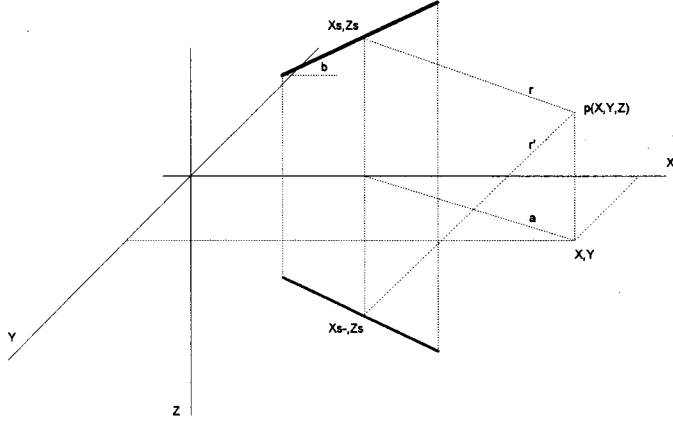


Fig. 3. Coordinate system.

$$\dot{A}_Z = \frac{\mu_m}{4\pi} \int_L \left\{ \text{sen } \beta \left[(g_m - g'_m) \delta_{mn} + V + \cos \beta \frac{\partial W}{\partial X} \right] \right. \\ \left. \cdot \dot{I} dl \right\} \quad (19)$$

where $g_m = e^{-\dot{\gamma}_m r} / r$ represents Green's function for the medium m and U, V, W represent Sommerfeld's integrals, that is:

$$U = \int_0^\infty \frac{2\lambda \mu_i J_0(\lambda a) e^{-(\dot{\alpha}_n |Z_s| + \dot{\alpha}_m |Z|)}}{\dot{\alpha}_1 \mu_2 + \dot{\alpha}_2 \mu_1} d\lambda \quad (20)$$

$$V = \int_0^\infty \frac{2\lambda \dot{\sigma}_j J_0(\lambda a) e^{-(\dot{\alpha}_n |Z_s| + \dot{\alpha}_m |Z|)}}{\dot{\alpha}_1 \dot{\sigma}_2 + \dot{\alpha}_2 \dot{\sigma}_1} d\lambda \quad (21)$$

$$W = \int_0^\infty \frac{2\lambda (\dot{\sigma}_2 \mu_2 - \dot{\sigma}_1 \mu_1) J_0(\lambda a) e^{-(\dot{\alpha}_n |Z_s| + \dot{\alpha}_m |Z|)}}{(\dot{\alpha}_1 \mu_2 + \dot{\alpha}_2 \mu_1)(\dot{\alpha}_1 \dot{\sigma}_2 + \dot{\alpha}_2 \dot{\sigma}_1)} d\lambda \quad (22)$$

where J_n are Bessel function of the first kind and n th order, and $\dot{\alpha}_k = \sqrt{\lambda^2 - \dot{\gamma}_k^2}$.

From expression of vector potential generated by a generic inducing segment calculated in some points along the induced conductor axis, the mutual inductive coupling coefficient can be computed by numerical integration of (8).

IV. THE SHIFTING COMPLEX IMAGES

Sommerfeld's integrals computation is in general rather onerous and in any case it requires numerical procedures. Nevertheless, introducing appropriate hypothesis, these integrals can be written as function series and then computed in approximate way.

Air and soil permeability can be considered constant and equal to that of the vacuum. Furthermore, at low frequency and accounting for electrical characteristics of soil and air, we can assume that $|\dot{\alpha}_2 \dot{\sigma}_1| \gg |\dot{\alpha}_1 \dot{\sigma}_2|$.

By introducing such approximations and considering the four possible combinations obtained changing source and observation point position it follows:

$$U \cong \int_0^\infty \frac{2\lambda J_0(\lambda a) e^{-(\dot{\alpha}_n |Z_s| + \dot{\alpha}_m |Z|)}}{\dot{\alpha}_1 + \dot{\alpha}_2} d\lambda \quad (23)$$

$$V \cong \frac{\dot{\sigma}_j}{\dot{\sigma}_1} \int_0^\infty \frac{2\lambda J_0(\lambda a) e^{-(\dot{\alpha}_2 |Z_s| + \dot{\alpha}_m |Z|)}}{\dot{\alpha}_2} d\lambda \quad (24)$$

$$W \cong - \int_0^\infty \frac{2\lambda J_0(\lambda a) e^{-(\dot{\alpha}_n |Z_s| + \dot{\alpha}_m |Z|)}}{(\dot{\alpha}_1 + \dot{\alpha}_2) \dot{\alpha}_2} d\lambda. \quad (25)$$

Such integrals can be approximated starting from following expressions [10]:

$$\int_0^\infty J_0(\lambda a) \frac{\lambda e^{-\sqrt{\lambda^2 - \dot{\gamma}^2} Z}}{\sqrt{\lambda^2 - \dot{\gamma}^2}} d\lambda = \frac{e^{-\dot{\gamma} r}}{r} \quad (26)$$

$$\int_0^\infty J_0(\lambda a) \frac{e^{-\sqrt{\lambda^2 - \dot{\gamma}^2} Z}}{\sqrt{\lambda^2 - \dot{\gamma}^2}} d\lambda = I_0 \left[\frac{\dot{\gamma}}{2} (r - Z) \right] K_0 \left[\frac{\dot{\gamma}}{2} (r + Z) \right] \quad (27)$$

where $r = \sqrt{a^2 + Z^2}$ and where $a = \sqrt{(X - X_s)^2 + (Y - Y_s)^2}$ indicates the horizontal projection of the distance between source and observation point.

Furthermore to calculate Sommerfeld's integrals it is useful to introduce the equivalent coefficient of propagation:

$$\dot{\gamma}_e = \frac{\dot{\gamma}_n (|Z| \delta_{mn} |Z_s|) + \dot{\gamma}_m (|Z| + |Z_s| \delta_{mn})}{(|Z| + |Z_s|)(1 + \delta_{mn})}. \quad (28)$$

For example equation (23) can be approximated starting from (26): for this purpose it is necessary to expand the exponential in a series of functions as follows:

$$\frac{2e^{-(\dot{\alpha}_n |Z_s| + \dot{\alpha}_m |Z|)}}{\dot{\alpha}_1 + \dot{\alpha}_2} = \sum_{i=1}^\infty \dot{a}_i \frac{e^{-\dot{\alpha}_e \dot{b}_i}}{\dot{\alpha}_e} \quad (29)$$

where $\dot{\alpha}_e = \sqrt{\lambda^2 - \dot{\gamma}_e^2}$. Then, the Sommerfeld's integral (23) can be written in the form:

$$U \cong \sum_{i=1}^\infty \dot{a}_i \frac{e^{-\dot{\gamma}_e \sqrt{a^2 + \dot{b}_i^2}}}{\sqrt{a^2 + \dot{b}_i^2}} = \sum_{i=1}^\infty \dot{a}_i \frac{e^{-\dot{\gamma}_e \dot{r}_i}}{\dot{r}_i} \quad (30)$$

where $\dot{r}_i = \sqrt{a^2 + \dot{b}_i^2}$.

In a similar way it is possible to approximate integrals V and W starting from equation (26) and (27), respectively. We obtain:

$$V \cong 2 \frac{\dot{\sigma}_j}{\dot{\sigma}_1} \sum_{i=1}^\infty \dot{a}_i \frac{e^{-\dot{\gamma}_e \sqrt{a^2 + \dot{b}_i^2}}}{\sqrt{a^2 + \dot{b}_i^2}} = 2 \frac{\dot{\sigma}_j}{\dot{\sigma}_1} \sum_{i=1}^\infty \dot{a}_i \frac{e^{-\dot{\gamma}_e \dot{r}_i}}{\dot{r}_i} \quad (31)$$

$$W \cong - \sum_{i=1}^k \dot{a}_i I_0 \left[\frac{\dot{\gamma}_e}{2} (\dot{r}_i - \dot{b}_i) \right] K_0 \left[\frac{\dot{\gamma}_e}{2} (\dot{r}_i + \dot{b}_i) \right]. \quad (32)$$

Every term of the summation corresponds to a image order. The subscript i indicates the order of images: longitudinal current and location of these images are defined by complex coefficients \dot{a}_i and \dot{b}_i respectively.

Such coefficients can be calculated only by a numerical routine. The set of coefficients can be obtained and optimized using a specific computer routine after having decided the maximum number of images to consider.

The greater the image order the lower is its contribution either because the distance between image and observation point increases or because the longitudinal current of the image reduces.

Therefore, the maximum image order to consider is limited. It is interesting to remark that the coefficient \dot{b}_i corresponds to the vertical distance between image and observation point (according to Z axis). Such distance is generally complex.

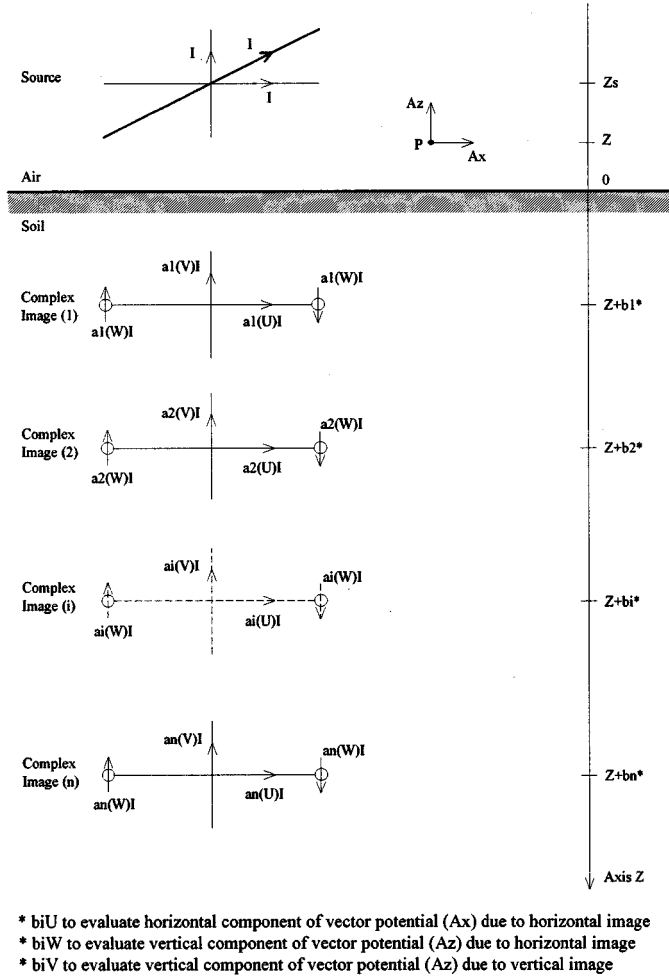


Fig. 4. Shifting Complex Images position Source and observation point in the air.

Images location is then defined in a coordinate system which has two real axis lying on the plane Σ and a third complex axis perpendicular to the same plane.

If the observation point changes, images move along the complex axis. The images motion is such that the complex distance between image and observation point, according to Z axis, remains always \dot{b}_i . Hence it follows the name of Shifting Complex Images Method (SCIM) assigned to this numerical method.

The Shifting Complex Images contains information about soil reaction to electromagnetic field. Therefore it is correct to place them in the soil.

It is possible and useful to give a graphical representation about the situations in the different and possible case, namely in the four possible combinations obtained changing source and observation point position. For instance, Fig. 4 shows the case with source and observation point in the air.

V. ELECTRIC AND MAGNETIC FIELD

Scalar potential produced by an elementary source, which leaks uniformly a current \dot{S} , can be obtained by applying the well known Images Method (IM).

Using equation (16) and keeping the previous meaning for subscripts it is easy to obtain:

$$\dot{V} = \dot{\rho}_m \dot{S} [(1 - \dot{v} + \dot{v} \delta_{mn}) \Psi + \dot{v} \delta_{mn} \Psi'] \quad (33)$$

where Ψ' represents equation (15a) relatively to the source image.

The end point effect may be neglected to calculate the scalar potential. In fact, the resultant of these effects as evaluated for the whole system is zero.

The vector potential produced by an elementary source interested by a uniform longitudinal current \dot{I} , can be obtained by applying SCIM.

Combining (18) and (19) with expressions (30)–(32), the components of the vector potential can be rewritten

$$\begin{aligned} \dot{A}_X &= \mu_0 \dot{I} L \cos \beta \left[(\Psi - \Psi') \delta_{mn} + \sum_{i=1}^k \dot{a}_i \Psi_i \right] \quad (34) \\ \dot{A}_Z &= \mu_0 \dot{I} L \left\{ \cos \beta \sum_{i=1}^k \dot{a}_i \Xi_i + \text{sen } \beta \right. \\ &\quad \cdot \left. \left[(\Psi - \Psi') \delta_{mn} + 2 \frac{\dot{\sigma}_j}{\dot{\sigma}_1} \sum_{i=1}^k \dot{a}_i \Psi_i \right] \right\} \quad (35) \end{aligned}$$

where

$$\begin{aligned} \Xi_i &= \frac{1}{4\pi L \cos \beta} \left\{ I_0 \left[\frac{\dot{\gamma}_e}{2} (\dot{r}_{ti} - \dot{b}_i) \right] K_0 \left[\frac{\dot{\gamma}_e}{2} (\dot{r}_{ti} + \dot{b}_i) \right] \right. \\ &\quad \left. - I_0 \left[\frac{\dot{\gamma}_e}{2} (\dot{r}_{ri} - \dot{b}_i) \right] K_0 \left[\frac{\dot{\gamma}_e}{2} (\dot{r}_{ri} + \dot{b}_i) \right] \right\}. \quad (36) \end{aligned}$$

Equations (34) and (35) provide the contribution of real sources and complex images sources to the vector potential.

The value of longitudinal and leakage currents of every elementary source computed by IM and SCIM enables to calculate the electric and magnetic field at any point in the surrounding medium as vectorial superposition of effects due to the elementary sources.

In a medium composed by two homogeneous isotropic and linear half spaces separated by a plane Σ , the electric field is generally expressed by (4a) where the scalar and vector potential are given by expressions written above:

$$\begin{aligned} \dot{\mathbf{E}} &= -\text{grad} \sum_{i=1}^n \dot{\rho}_m \dot{S}_i [(1 - \dot{v} + \dot{v} \delta_{mni}) \Psi_i + \dot{v} \delta_{mni} \Psi'_i] \\ &\quad - j\omega \sum_{i=1}^n (\dot{\mathbf{A}}_{Xi} + \dot{\mathbf{A}}_{Zi}). \quad (37) \end{aligned}$$

Similarly magnetic field is given by (4b).

Rearranging (4b) together with expressions (34) and (35) lead to the following equation:

$$\dot{\mathbf{H}} = \frac{1}{\mu} \text{rot} \sum_{i=1}^n (\dot{\mathbf{A}}_{Xi} + \dot{\mathbf{A}}_{Zi}). \quad (38)$$

Equations (37) and (38) take into account the contribution of both real sources and image sources defined from IM and SCIM.

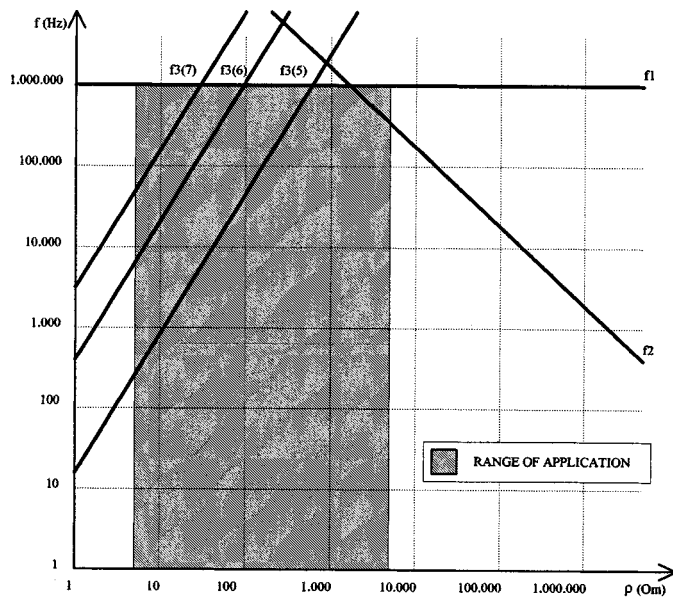


Fig. 5. Range of application of the computing code AGSA.

VI. RANGE OF APPLICATION OF THE METHOD

The methodology illustrated above has been implemented in a computer program called AGSA (Aerial and Grounding System Analysis).

Limit of AGSA application are due both to initial hypothesis and to simplifications assumed for computing the Sommerfeld's integrals. Most important limits are:

$$f_1 \leq 10^6 \quad (39)$$

because Sommerfeld's integral have not been considered in the calculation of electrostatic field [2];

$$f_2 \leq 1/20\pi\rho_1\varepsilon_0 \quad (40)$$

in order the magnitude of soil complex conductivity to be much greater than that of the air;

$$f_3(k) \leq (g_k^2\rho_1)/(2\pi\mu_0) \quad (41)$$

(where g_k depends on the number k of the complex images taken into account) in order to keep the propagation constant of the soil sufficiently small.

The range of application of AGSA can be graphically represented as shown in Fig. 5.

AGSA covers the usual application in electric power systems. The frequency range of application includes sub-synchronous, synchronous, harmonic and free evolution state. In terms of resistivity, the field of application ranges from values typical of sea water to values pertinent to rocky and dry soil and higher.

AGSA is useful to carry out analysis only in the frequency domain. However, it is always possible to change from time-domain to frequency domain by applying Fast Fourier Transformation (FFT).

As well known by this mathematical transformation an input transient signal can be decomposed in a set of single-frequency signals. After the decomposition, the time-response of a generic

conductors system can be obtained first by the application of AGSA to every single-frequency signal and then by using the inverse Fast Fourier Transformation to return in the time domain.

The response to a single-frequency signal is computed for a range of frequencies starting from 0 up to Nyquist frequency f_{\max} given by the following equation:

$$f_{\max} = \frac{1}{2\Delta t} \quad (44)$$

where Δt denotes the earliest time for which accurate information on a response are desirable (assuming that the excitation current is also known at that time).

A transfer function $W(j\omega)$ of the conductor system is obtained for each component included in the FFT of the input signal.

If $x(t)$ represent the input signal and $y(t)$ the response, then:

$$y(t) = F^{-1}\{W(j\omega)F[x(t)]\} \quad (45)$$

where F and F^{-1} are the Fourier and inverse Fourier transforms respectively.

Obviously this procedure is suitable only if the propagation medium (air and soil) and the source system exhibits linear characteristics for each single frequency considered. For each frequency it is possible to take into account different values of the electrical characteristics of medium and sources. This is important because normally these characteristics (in particular way of the soil) depend on frequency. This dependence is due to the reduction of the time available for the polarizing charges to separate and participate in the current conduction as the frequency raised from a low value to the MHz range. It is not easy to include this frequency dependence in a time domain approach. On the contrary, using a frequency domain method it is easy to cater for any frequency dependence of each electrical characteristic.

The frequency range of application of AGSA covers the frequency spectrum of a typical full lightning. Therefore by using AGSA and Fourier Transform according to the procedure just described it is possible to analyze the behavior of a generic conductor system energized by a lightning.

Indeed, in this case to obtain right results it is necessary to consider that the apparent resistivity of an homogeneous isotropic soil is constant as long as the magnitude of electric field remains below a specific value. Over this value, because soil ionization mechanism, the soil apparent resistivity decreases.

Further analysis are necessary to develop a method which take into account this phenomena.

VII. APPLICATION TO SOME SIMPLE PROBLEMS

We consider situations illustrated in Fig. 6.

- A) overhead short conductors
- B) buried short conductors
- C) vertical conductor through the earth surface

A. Overhead Short Conductor Energized at Both Extremities

Figs. 7 and 8 represent magnetic field generated by vertical and horizontal short overhead conductors as shown in Fig. 6(a). Conductors are energized by a double injection current of 1 A at

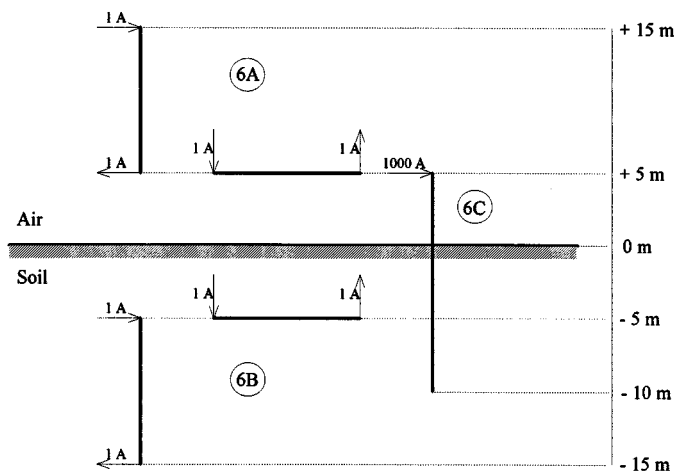


Fig. 6. Cases analyzed.

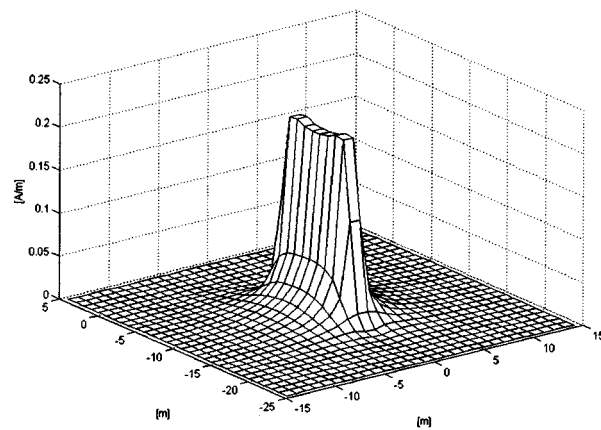


Fig. 9. Magnetic field distribution due to a vertical conductor.

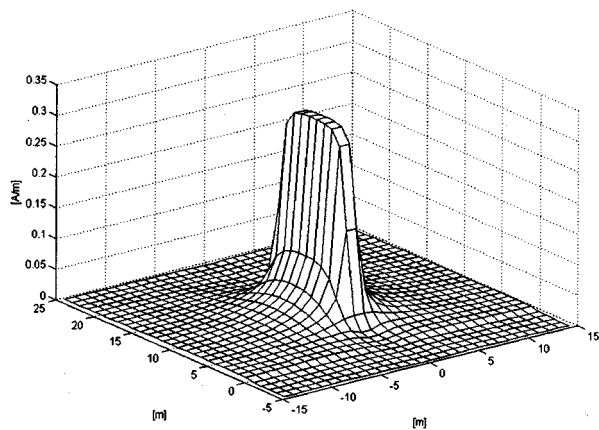


Fig. 7. Magnetic field distribution due to a vertical conductor.

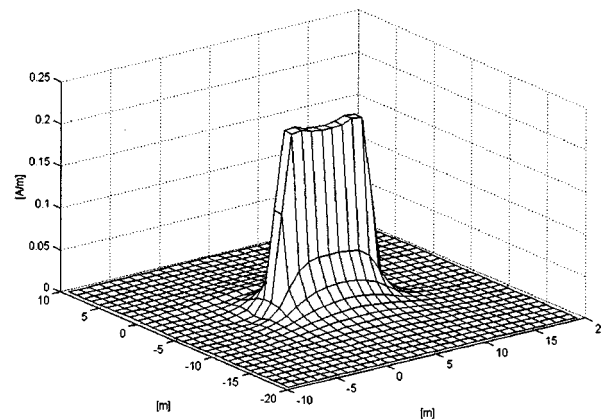


Fig. 10. Magnetic field distribution due to an horizontal conductor.

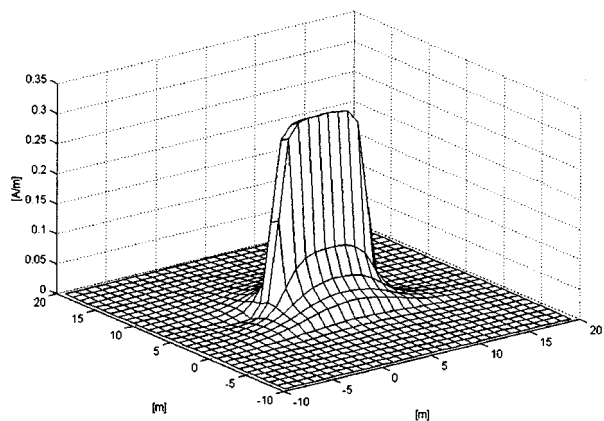


Fig. 8. Magnetic field distribution due to an horizontal conductor.

1 MHz. Magnetic field is computed on a vertical surface which contains the source and through the earth surface. The computational step, along two axis, is 1 m.

As well known the distribution of the magnetic field is closely related to the distribution of the longitudinal current along the conductor. Since the source is embedded in a nonconductive medium (air), the current along the conductor remains practically uniform.

Thus, the magnetic field reaches the same value along the whole development of the segment whereas it decreases when the distance of the observation point from the source increases.

The maximum value of the magnetic field represented in Figs. 7 and 8 corresponds to a minimum distance of 0.5 m from the source: the actual maximum value is reached on the segment surface and depends on the conductor radius.

Obviously, continuity conditions for tangential component of magnetic field must be satisfied at the earth surface.

Furthermore the magnetic field decrease faster in the soil because the skin depth in the soil is greater than in the air.

1) *Buried Short Conductor Energized at Both Extremities*: If a conductor is embedded in a conductive medium, like soil its behavior changes respect to the previous case because the earth leakage current is now not negligible. This phenomena due to internal impedance of the conductor is obviously more evident at high frequencies.

Figs. 9 and 10 represent magnetic field generated by vertical and horizontal short buried conductors like shown in Fig. 6(b) respectively. Energization and computation surfaces are the same of the previous case. With regard to continuity conditions and to skin depth, consideration made in the previous case are still valid.

2) *Buried Short Conductor Energized at One Extremity*: Figs. 11–14 represent magnetic and electric fields

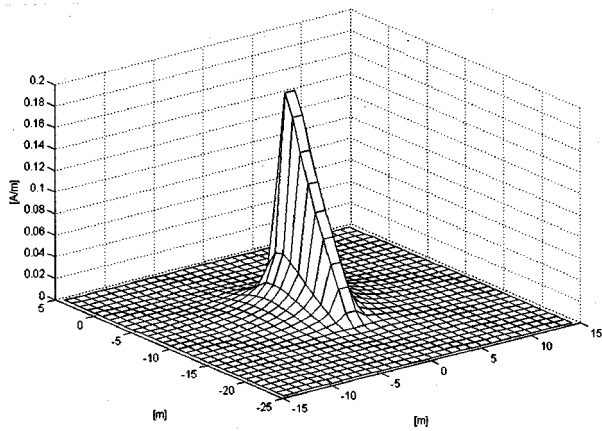


Fig. 11. Magnetic field distribution due to a vertical conductor.

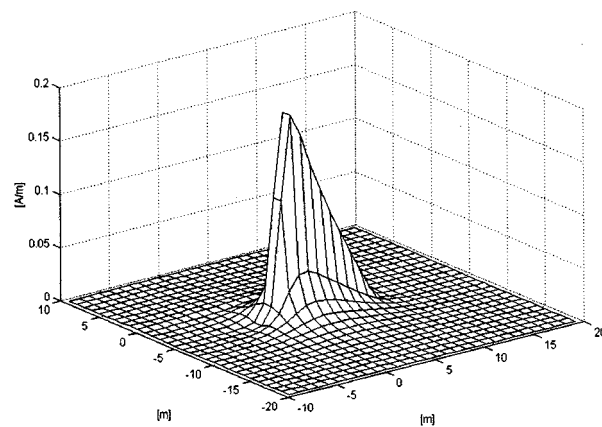


Fig. 12. Magnetic field distribution due to an horizontal conductor.

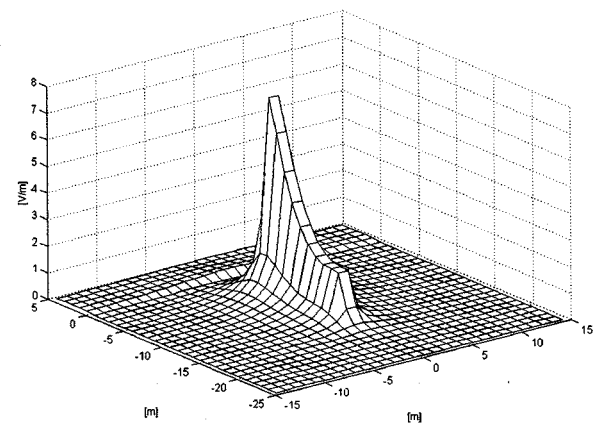


Fig. 13. Electric field distribution due to a vertical conductor.

generated by vertical and horizontal short buried conductors like shown in Fig. 6(b) respectively. In this case conductors are energized by a single injection current of 1 A at 1 MHz.

The return of the current is assumed to be at a remote electrode. Calculation surfaces are the same of the previous cases.

The whole injected current flow into earth. Magnetic and electric field near the source are representative of the distribu-

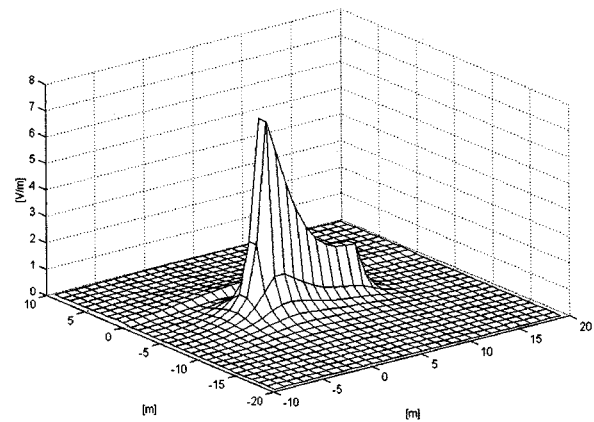


Fig. 14. Electric field distribution due to an horizontal conductor.

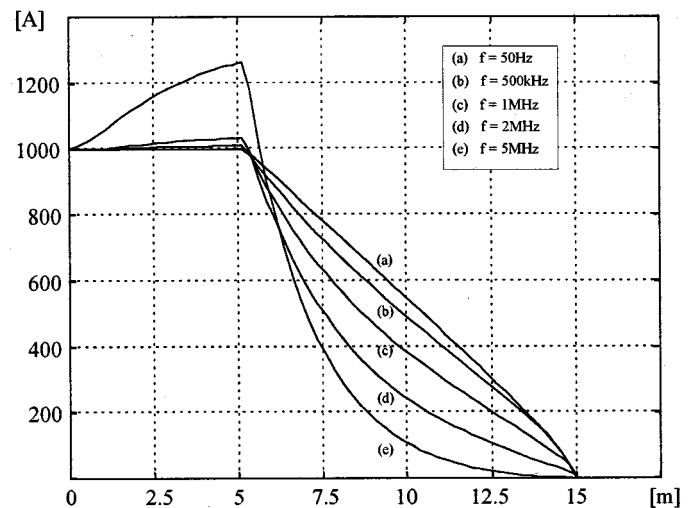


Fig. 15. Longitudinal current distribution along the conductor at different frequencies.

tion of the longitudinal and leakage current along the conductor respectively.

As regards to continuity conditions for tangential components of electric and magnetic field at the earth surface and to skin depth, considerations made in the case (A) are still valid.

Further information about current distribution along buried conductor are given in the next section.

B. Vertical Conductor Energized at One Extremity

Fig. 15 shows longitudinal current profiles along the conductor represented in Fig. 6(c) at different frequencies. In all cases the current injected at the top end of the segment is 1000 A.

It is interesting to observe how the distribution of the longitudinal current changes, in the overhead and buried conductor portion, with frequency.

Longitudinal current profile in the overhead part remains uniform up to frequencies of about 1 MHz. This behavior was expected since air is a nonconductive media. At higher frequencies the behavior of the above ground conductor can be explained by solving classic wave equations which describe completely the sinusoidal state of transmission line: the wavelength associated to sinusoidal state of the system became comparable to the

length of the above ground conductor (for instance at 5 MHz the wavelength of an overhead line is about 60 m).

In all cases, in the buried part of the conductor, longitudinal current profile decrease up to zero at the bottom end point.

At very low frequencies the leakage current is practically uniform because the effect of the internal impedance of the conductor is negligible. At higher frequencies the internal impedance of the conductor reaches such a value to make greater the earth leakage current density at the begin of the buried section. For this reason the slope of the longitudinal current profile increases with the frequency.

These computational results are successfully compared to that ones provided by other software packages (e.g., CDEGS).

Therefore it seems that AGSA can be used over 1 MHz (39). This limit, given by CCITT, is probably too prudent in this case.

VIII. CONCLUSIONS

A numerical method for the analysis of both aerial and buried system of conductors in wide frequency range has been described.

The method based on integral methods is advantageous, as compared with differential ones, to solve linear problems in open regions. To study a medium formed by two half spaces with different characteristics the well-known Images Method (IM) has been used and the Shifting Complex Images Method (SCIM) has been developed. These complex images derive from Sommerfeld's integral.

The range of application of the method has been specified: it can be applied up to 1 MHz covering the frequency range of usual interest in power systems.

Analytical developments have required considerable efforts. On the other hand this allows to obtain algorithms that reduce computation task.

Thus the computer program (AGSA) which implements the numerical method proposed in this paper can run on a normal Personal Computer. The generality of the approach assumed in this paper enables on the one hand to have a flexible computing code, on the other hand to incorporate into a single linear system both lumped circuit parameters and distributed parameters evaluated through a rigorous electromagnetic field analysis.

REFERENCES

- [1] S. A. Scheikunoff, "The electromagnetic theory of coaxial transmission lines and cylindrical shields," *The Bell System Technical Journal*.

- [2] CCITT, "Directives concernant la protection des lignes de télécommunication contre les actions nuisibles des lignes électriques," New Delhi, 1960.
- [3] "Directives concerning the protection of telecommunication lines against harmful effects from electric power and electrified railway lines," Geneva, vol. II e III, 1989.
- [4] A. Sommerfeld, "Ueber die Ausbreitung der Wellen in der drahtlosen Telegraphie," *Annalen der Physik*, vol. 28, pp. 665–736, 1909.
- [5] L. Grcev and F. Dawalibi, "An electromagnetic model for transients in grounding systems," *IEEE Transactions on Power Delivery*, vol. 5, no. 4, pp. 1773–1781, novembre 1990.
- [6] F. Dawalibi and A. Selby, "Electromagnetic fields of energized conductors," *IEEE Trans. Power Delivery*, vol. 8, no. 3, p. 1275, 1284, luglio 1993.
- [7] R. Andolfato, L. Bernardi, and L. Fellin, "A wide frequency range computation code for overhead and buried conductor system," in *8th ICHQP Proceedings*, Athens, Gr, ottobre 21–23, 1998, pp. 1064–1070.
- [8] E. D. Sunde, *Earth Conduction Effects in Transmission Systems*. New York, NY: D. Van Nostrand Company Inc., 1949.
- [9] R. F. Harrington, *Field Computation by Moment Methods*. Florida: R. E. Krieger publishing company, 1968.
- [10] M. Abramovitz and I. A. Stegun, *Handbook of Mathematical Functions*. New York, NY: Dover Publications Inc., 1970.

Roberto Andolfato received a dr.ing. and Ph.D. degree in electrical engineering from University of Padova respectively in 1990 and 1998. His main field of interest is power system earthing with specific emphasis at developing numerical procedures for simulating the electromagnetic field generated by complex geometry in dispersing media. He also is a Professional Consultant Engineer and a member of the Italian Electrical and Electronic Association (AEI).

Luca Bernardi received a dr.ing. degree in electrical engineering from University of Padova in 1997 and is actually attending his Ph.D. course at the same university. His branch of research is electromagnetic interference between electric power installations and other systems. He is also a member of the Italian Electrical and Electronic Association (AEI).

Lorenzo Fellin received a dr.ing. degree in electrical engineering from University of Padova in 1967. He joined the Electrical Engineering Dept. of the University of Padova in 1968 where, from 1986, he is Full Professor of Electric Power Installations. He was actively involved in the design and construction of a large laboratory for thermonuclear fusion research (the RFX experiment built-up in Padova with Euratom-ENEA-CNR support). His field of interests also include design of industrial electric installations and electric lighting design. He is a member of IEEE and of the Italian Electrical and Electronic Association (AEI). He also is one of the chairmen of the Italian Association of Artificial Lighting (AIDI).